Robotica (2007) volume 25, pp. 493–500. © 2007 Cambridge University Press
doi:10.1017/S0263574707003372 Printed in the United Kingdom

Development of a compact double-disk magneto-rheological fluid brake

Wei Zhou, Chee-Meng Chew* and Geok-Soon Hong

Department of Mechanical Engineering, National University of Singapore, 9, Engineering Drive 1, Singapore 117576, Singapore

(Received in Final Form: January 5, 2007. First published online: February 12, 2007)

SUMMARY

This paper describes the development of a novel compact magneto-rheological (MR) fluid brake with high transmitted torque and a simple structure. The MR fluid brake has two shearing disks with an electromagnetic coil located between them. Such a structure enables the brake to have a small radial dimension and a large torque transmission capacity. In the design process, a Bingham viscoplastic model is used to predict the transmitted torque. Electromagnetic finite element analysis (FEA) is performed to assist the magnetic circuit design and structural parameters' optimization. The novel brake design is prototyped and studied. Experimental results show that a compact MR fluid brake with high transmitted torque is successfully achieved.

KEYWORDS: Magneto-rheological (MR) fluid brake; High transmitted torque; Compact size; Bingham viscoplastic model; Finite element analysis (FEA).

1. Introduction

Magneto-rheological (MR) fluids belong to a class of intelligent materials, which respond to applied magnetic field with fast, continuous, and reversible change in their rheological behavior. MR fluids have attracted extensive research interest recently because they can provide simple, quiet, fast-response interface between electronic control and mechanical system.[3] A lot of work has been done on the MR fluids property investigation, and the modeling and control of MR fluid brakes.[4,12,16,21] A wide range of MR fluid brakes have also been investigated for their potential applications in various systems, such as, semiactive suspension systems, shock absorbers, vibration control, seismic response reduction, etc.[2,7,9,17]

MR fluid brakes have also been used in actuators due to their distinguished force control and power transmission features.[15,18,22] In our previous work, a MR fluid brake was employed to emulate a viscous damper in our proposed force control actuator system known as series damper actuator (SDA).[1,14] By applying a proper control effort, virtual viscous damping with large varying range could be achieved with the MR fluid brake. The SDA system requires the MR fluid brake to have a high transmitted torque, be compact in size, be lightweight, and allow 360° rotation, and so on. The properties of MR fluid brake determine the performance of the SDA system.

Currently, there are a lot of solutions for MR fluid brake design. Some MR fluid brakes have been developed and commercialized with attractive properties, such as high yield stress and stable behavior.[10] Furthermore, there are also a lot of research works on the design and implementation issues of MR fluid brake, as well as its counterparts—electro-rheological (ER) brake. Carlson[11] developed a controllable brake based on MR fluid. A rotary-type MR fluid damper using valve mode was introduced by Kim.[5] Li[6] designed and fabricated a highly efficient MR fluid brake with a simple structure. Kavlicoglu[9] has presented a high-torque MR fluid clutch design with double plates. A multiple disks ER brake has been proposed by Papadopoulos in ref. [8].

The objective of this work is to design and develop a novel MR fluid brake with high transmitted torque, yet being compact in size and lightweight. In this paper, a novel MR fluid brake structure with double shearing disks is presented. The general design procedures for the brake are also described. FEA simulation was performed to analyze the magnetic circuit and obtain optimized parameters for a prototype. The prototype of the proposed MR fluid brake was fabricated and studied. Experimental results are presented and discussed at the end of this paper.

2. Structural Design and Analysis of a MR Fluid Brake

2.1. Structure design

The main objective of this design is to achieve high brake torque for a given size. Most current solutions of MR fluid brake design are either low in transmitted torque or large in size. A typical structure of MR fluid brake is as shown in Fig. 1. It is a single disk type and operates in shear mode. The electromagnetic coil is located beyond the outer edge of the shearing disk in the brake. It generates magnetic flux penetrating the shearing disk and the MR fluid in the gap. Such configuration often results in a large radial dimension if high transmitted torque is to be achieved. Table I shows the specifications of a commercial MR fluid brake, MRB-2107-3 from Lord Corporation.

In Fig. 2, a schematic of our proposed MR fluid brake structure is shown. To reduce the size of the brake in this design, we shift the electromagnetic coil closer to the axis

*Corresponding author. E-mail: chewcm@alum.mit.edu

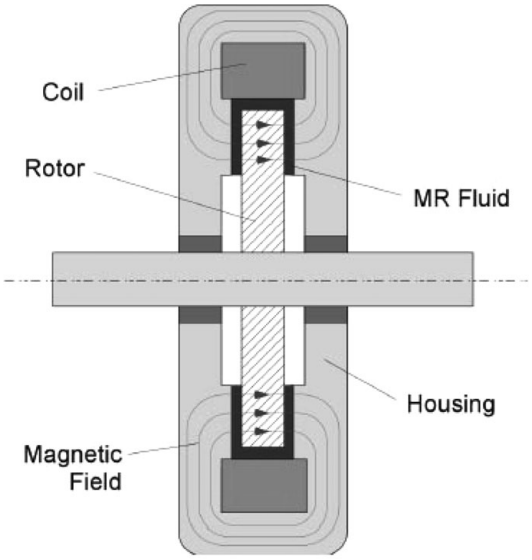

Fig. 1. A typical structure for MR fluid brakes (Lord Corp.).

Table I. The specifications of MRB-2107-3 MR fluid brake from Lord Corporation.

Maximum output	5.6 Nm
Diameter	92.2 mm
Length	36.6 mm
Weight	1410 g
Maximum input current	1 A
Maximum operating speed	1000 rpm

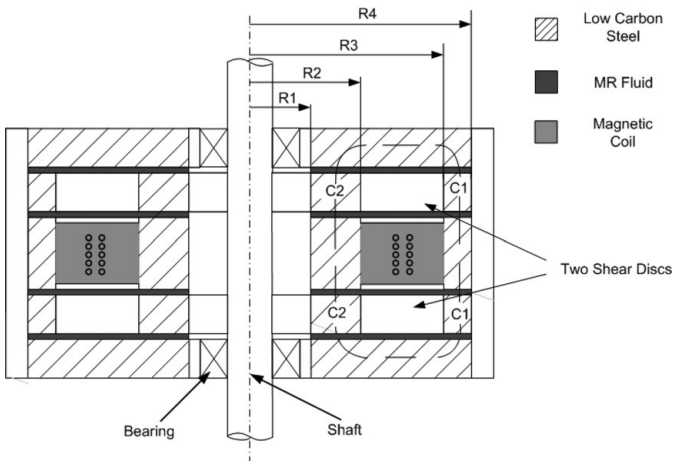

Fig. 2. A schematic drawing of proposed MR fluid brake structure.

of rotation and locate it on one side of the shear disk. To increase the torque transmission capacity, another shear disk is added on the other side of the electromagnet coil, forming a symmetrical structure. Such a design fully utilizes the radial dimension to generate high transmitted torque. The dashed line represents the magnetic flux path generated by the electromagnetic coil. There are two active shear zones for each disk. They are the outer and inner shear zones, labeled by C_1 and C_2, respectively. Since each disk has two shear surfaces, there are altogether eight shear areas in the system.

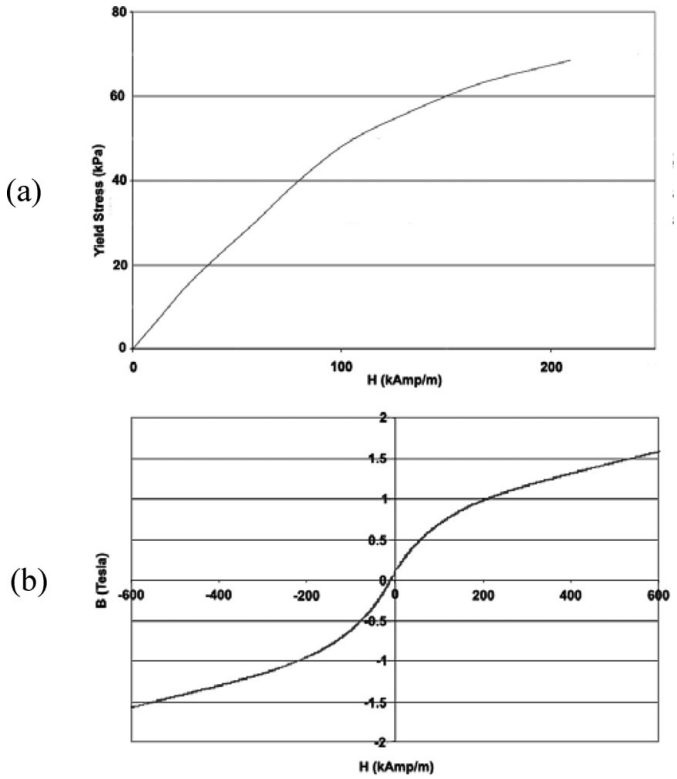

Fig. 3. Rheological and magnetic properties of MR fluid (MRF-241ES from Lord Corp.). (a) Yield stress versus magnetic field strength. (b) Magnetic flux density versus magnetic field strength.

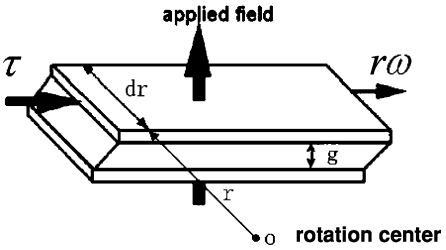

Fig. 4. The direct shear mode of MR fluid devices.

2.2. *Bingham viscoplastic model and shear mode torque*

MR fluid has a magnetic field-dependent rheological property. The magnetic field can dramatically change the viscosity of the fluid. For example, the rheological and magnetic properties of a commercial MR fluid (MRF-241ES from Lord Corp.) are shown in Fig. 3.

The behavior of MR fluid is often represented by Bingham viscoplastic model.[12] The constitutive equation for the model is as follows:

$$\tau = \tau_y(H)\mathrm{sgn}(\dot{\gamma}) + \eta\dot{\gamma} \tag{1}$$

where τ is the shear stress, τ_y is the field dependent yield stress of the MR fluid (Fig. 3a), H is the magnetic field strength, $\dot{\gamma}$ is the shear rate, η is the plastic viscosity (i.e., viscosity at $H = 0$). The first part of the RHS of Eq. (1) is the yield stress produced by the magnetic field and the second part is the shear stress obtained from the fluid viscosity.

The designed brake is operated in direct shear mode as shown in Fig. 4. In this operation mode, the shear stress

https://doi.org/10.1017/S0263574707003372 Published online by Cambridge University Press

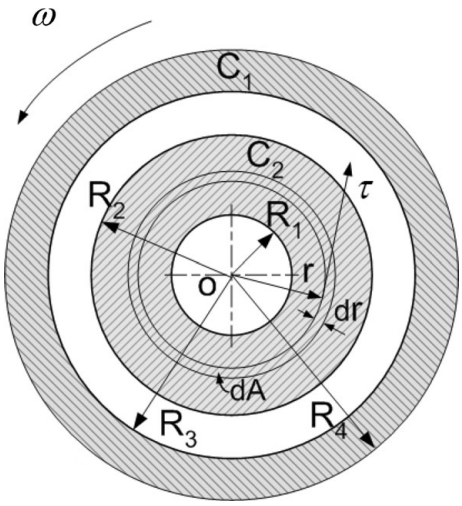

Fig. 5. Active shear area on the shearing disk.

developed, τ, is:

$$\tau = \tau_y \operatorname{sgn}(\omega) + \frac{\eta \omega r}{g} \tag{2}$$

where ω is the rotary shear speed, γ is the distance to the rotation center, and g is the gap between the two shear surfaces.

In this brake design as shown in Fig. 2, there are two shear disks, each having two shear zones (C_1 and C_2). The active shear area on one disk is shown in Fig. 5, where ω is the angular velocity of each disk with respect to the structure, dA is the area of the small circular area with radius r and small radial increment dr, and R_1 and R_2 and R_3 and R_4 are inner and outer radii of the two shearing zones C_1 and C_2, respectively. According to Eq. (2), the generated torque can be written as:

$$\begin{aligned} T &= \int_{C_1+C_2} r\tau \, \mathrm{d}A \\ &= 2\pi \int_{R_1}^{R_2} \left(\tau_y r \operatorname{sgn}(\omega) + \frac{\omega \eta r^2}{g} \right) r \, \mathrm{d}r \\ &\quad + 2\pi \int_{R_3}^{R_4} \left(\tau_y r \operatorname{sgn}(\omega) + \frac{\omega \eta r^2}{g} \right) r \, \mathrm{d}r. \end{aligned} \tag{3}$$

Note that the yield stress τ_y in the two shear areas, C_1 and C_2, may not be equal. Assume that the yield stresses in C_1 and C_2 are τ_{y1} and τ_{y2}, respectively. Equation (3) can then be rewritten as:

$$\begin{aligned} T &= \frac{2}{3}\pi \left[\tau_{y1} \left(R_2^3 - R_1^3 \right) + \tau_{y2} \left(R_4^3 - R_3^3 \right) \right] \operatorname{sgn}(\omega) \\ &\quad + \frac{\pi \eta \omega}{2g} \left[\left(R_2^4 - R_1^4 \right) + \left(R_4^4 - R_3^4 \right) \right]. \end{aligned} \tag{4}$$

Equation (4) is the shear torque generated on one surface of a shear disk. In this design, there are two shearing disks and hence four shear surfaces. That is, the effective torque for such a brake design is given by 4T.

2.3. Magnetic circuit design

In our design, the electromagnetic coils are located between the two shear disks. By applying current through the coils, magnetic flux is generated along a closed path (dash line) as shown in Fig. 2. The flux penetrates the gaps along the flux path, and therefore changes the yield stress of the MR fluid in those gaps. The target of magnetic circuit design is to determine the magnetic circuit excitation, NI (A · turns), which can give the desired yield stress (τ_y) of the MR fluid in the gaps. The general steps for magnetic circuit design are described as follows.

Step 1. The operation point (H_f, B_f) of MR fluid

The operation point of MR fluid is defined as the magnetic field strength, H_f, and flux density, B_f, of the MR fluid in the shear gap, when the desired shear stress is obtained. According to this definition, H_f can be found from the $\tau_y - H$ curve of the MR fluid (Fig. 3a), given the desired yield stress, τ_y. Thereafter, the magnetic flux density B_f can be determined from B–H curve of the MR fluid (Fig. 3b). Alternatively, if a linear relationship between B and H is approximated for the material, the flux density can be calculated as:

$$B = \mu_0 \mu_r H \tag{5}$$

where $\mu_0 = 4\pi \times 10^{-7}\mathrm{T}/(\mathrm{A} \cdot \mathrm{turns})$ is the vacuum permeability and μ_r is the relative permeability of flux path material.

Step 2. The operation point (H_s, B_s) of steel

According to the principle of continuity of magnetic flux and assuming no flux leakage, we have:

$$\Phi_s = \Phi_f \tag{6}$$

where Φ_s are Φ_f are the magnetic flux in steel path and fluid gap, respectively; and,

$$\Phi_s = B_s A_s \tag{7}$$

$$\Phi_f = B_f A_f \tag{8}$$

where B_s and B_f are the flux density in the steel path and the fluid gap, respectively; A_s and A_f are the cross-sectional area of the steel path and the fluid gap, respectively.

Therefore, the flux density in the steel path B_s can be expressed as:

$$B_s = \frac{B_f A_f}{A_s}. \tag{9}$$

Thereafter, the magnetic field strength in the steel path, H_s, can be found from the B–H curve of the steel material or from Eq. (5). A typical B–H curve of steel is shown in Fig. 6.

Step 3. Magnetic circuit excitation, NI (A·turns)

Applying the magnetic circuit principle[19] gives:

$$NI = H_f g + H_s L \tag{10}$$

https://doi.org/10.1017/S0263574707003372 Published online by Cambridge University Press

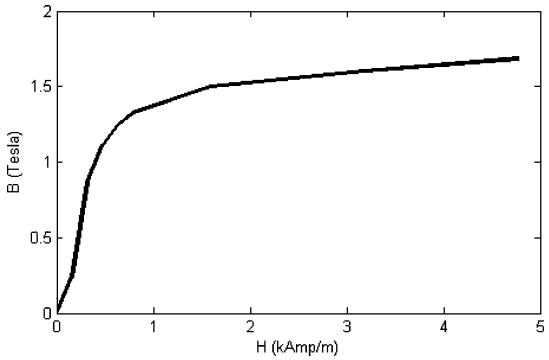

Fig. 6. A typical *B–H* curve of steel.

where N is the number of coil turns, I is the coil current, g is the gap length, and L is the length of the steel path.

If there are n MR fluid gaps and m steel path sections series connected in the closed magnetic circuit, then Eq. (10) can be written as:

$$NI = \sum_{i=1}^{n} H_{if} g_i + \sum_{j=1}^{m} H_{js} L_j \tag{11}$$

where H_{if} is the H_f in ith fluid gap and H_{js} is the H_s in jth steel path.

Because the relative permeability (μ_r in Eq. (5)) of steel is far larger than that of MR fluid, the magnetic field strength in steel H_s is usually much lower than that in MR fluid gap H_f, that is $\sum_{j=1}^{m} H_{js} L_j$ can be neglected and Eq. (11) can be simplified as follows:

$$NI = \sum_{i=1}^{n} H_{if} g_i. \tag{12}$$

If all the MR fluid gaps have the same gap length, g, and magnetic field strength, H_f, this equation can be further simplified as follows:

$$NI = n H_f g. \tag{13}$$

These equations enable the designers to estimate the required magnetic circuit excitation, NI (A·turns), given required magnetic field strength and flux path dimensions. However, getting an accurate magnetic circuit design using the method described earlier is very difficult due to the nonlinear properties of materials (see Figs. 3 and 6) and some other nonidealities, such as flux leakage and flux path dimension uncertainties. Finite element analysis software is used to aid the optimization process of the magnetic design. The three steps of the magnetic circuit design described earlier should be performed before the FEA analysis and optimization. Although the calculated magnetic circuit excitation, NI, may not be accurate, it can be used as an initial condition for the FEA analysis and then adjusted accordingly.

2.4. *FEA analysis and design optimization*

Electromagnetic finite element analysis is performed in this work to assist the electromagnetic circuit design and optimize the brake's structural parameters. The FEA simulation software used in this work is the 2D Maxwell from ANSOFT.[13]

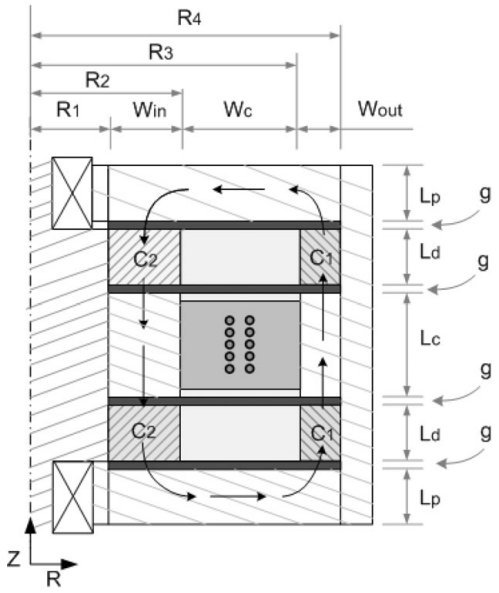

Fig. 7. The 2D FEA model of the designed double disks MR fluid brake.

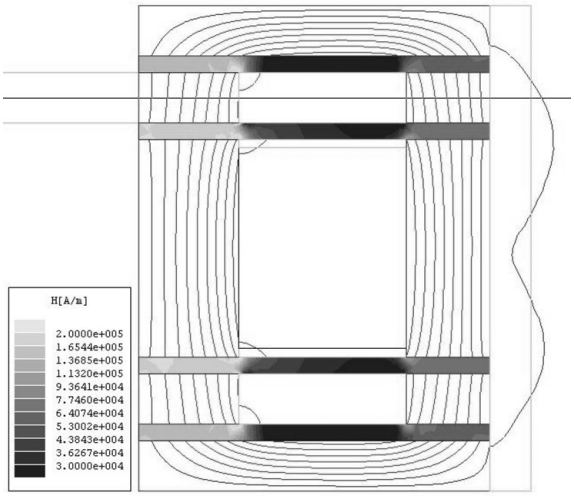

Fig. 8. An example of the FEA simulation results.

The FEA 2D model geometry (in the RZ plane of a cylindrical coordinate system) is shown in Fig. 7. The model is actually a 3D axisymmetric object. The 2D model represents a 3D structure that has been revolved around the axis of symmetry (Z axis). 2D Maxwell analyzes the 2D geometry as a cross-section of the model and generates a solution for that cross-section.

An example of the FEA simulation result is shown in Fig. 8. The magnetic flux (the closed curves) and the gap magnetic field strength (gray scale) are displayed in the result. The magnetic path is clearly indicated by the flux lines. Some flux leakage can be observed. From the simulation result, the magnetic field strength in all the eight MR fluid gaps can be obtained. The generated shearing torque can be calculated according to Eq. (4). The simulation results, therefore, can be used to evaluate the magnetic circuit design described in

https://doi.org/10.1017/S0263574707003372 Published online by Cambridge University Press

the previous subsection. The magnetic circuit excitation, NI, can be adjusted till satisfactory yield stresses in these gaps are obtained. Furthermore, the FEA analysis results can also be used to evaluate the brake structural design and optimize its dimensional parameters.

Although the magnetic strength distribution in the radial direction of each gap is supposed to be uniform, it is actually not uniform as indicated in the simulation results. Estimated average value is reasonable to be used here to represent the uniform magnetic field strength in each gap. In the simulation of Fig. 8, the magnetic circuit excitation, NI, is 10^3 A · turns, the gap length, g, is 1 mm, and the magnetic field strength, H_{if}'s, in the eight gaps, according to the simulation result, are estimated to be: 1.8×10^5 A/m, 1.8×10^5 A/m, 1.6×10^5 A/m, 1.6×10^5 A/m, 0.8×10^5 A/m, 0.8×10^5 A/m, 0.6×10^5 A/m, 0.6×10^5 A/m. That is, $\sum_{i=1}^{8} H_{if} g_i = 9.6 \times 10^2$ A · turns. It can be seen that the simulation result is quite close to the theoretical one according to Eq. (12).

Important parameters have also been indicated in Fig. 7, where

R_1 and R_2 and R_3 and R_4 are the inner and outer radii of the two shearing areas C_1 and C_2, respectively;
L_p is the thickness of the side steel path;
L_d is the thickness of the shearing disk;
L_c and W_c are the length and width of the magnetic coil, respectively;
W_{in} and W_{out} are the width of the inner and outer steel paths, respectively; and
g is the MR fluid gap length.

R_4 and R_1 decide the active shear area of the MR fluid. To obtain large torque transmission capability, large R_4 and small R_1 is always preferred. R_4 can be determined according to the maximum permitted brake size, usually, from the design requirements. R_1 can be determined from the minimum shaft size required from the aspects of component strength, manufacturing and assembling, and so on. Satisfying the disk strength and manufacturing requirements, the thickness of the shearing disk, L_d, should be as small as possible to reduce the weight and size of the brake and lower the flux strength loss in the steel path. L_c and W_c can be determined by considering the wire diameter and the required number of turns for the magnetic coil.

The selection of the structural parameters, g, L_p, W_{in}, and W_{out}, is briefly discussed as follows.

- *Gap Length, g*

According to Eq. (11), the gap length, g, is known to significantly affect the magnetic field strength, H. A simulation result of the relationship between the gap length and the magnetic field strength in this gap is shown in Fig. 9. It can be seen that a smaller gap gives a larger magnetic field strength. Generally, a larger magnetic field strength will result in a larger yield stress for the MR fluid and, consequently, generate a larger transmitted torque. If the MR fluid operation points are given, smaller gap always means lower value is needed for NI (A · turns). In this sense, a smaller gap will be better. However, the lower value for the gap length is limited by the manufacturing considerations

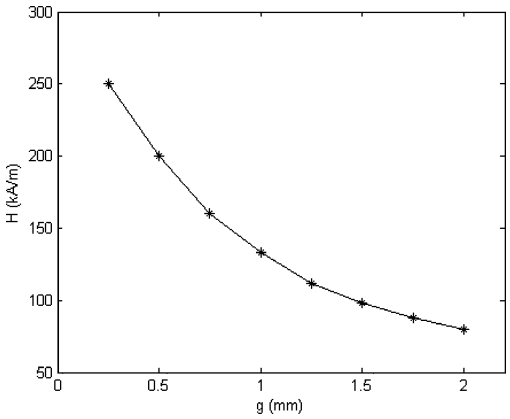

Fig. 9. A simulation result for the gap length, g, versus the magnetic field strength, H, in this gap.

and assembling errors. Furthermore, the smaller the gap is, the more sensitive the magnetic field strength, H, is to the gap length errors (see Fig. 9). Usually, the gap length is between 0.25 and 2 mm for ease of manufacturing and assembly.[6,20] In this design, the gap is set to 1 mm.

- *Width of inner and outer flux path, W_{in} and W_{out}*

W_{out} and W_{in} are the radial width of the shear areas C_1 and C_2, respectively. They also represent the width of the outer and inner flux path, respectively. When R_1, R_4, and W_c are given, the summation of W_{in} and W_{out} will be fixed because:

$$W_{in} + W_{out} = R_4 - R_1 - W_c. \tag{14}$$

Therefore, increasing W_{in} will decrease W_{out}, and vice versa. W_{out} and W_{in} will determine the areas of the two shear regions C_1 and C_2. Larger area of C_1 may be preferred since it is at larger radius than C_2 and therefore may result in higher transmitted torque. However, large W_{out} will result in a small shear area for C_2. Furthermore, a small W_{in} may result in magnetic saturation in the inner steel path. When the magnetic path is saturated, the path flux density would not have significant response to the change of magnetic circuit excitation. Consequently, the magnetic field strength in the outer MR fluid gaps would be limited to a relatively low level. The optimal values for W_{in} and W_{out}, which will result in large, transmitted torque can be obtained by the use of FEA simulation.

A simulation result is presented in Fig. 10, which shows the effect of different values of W_{in} and W_{out} on the transmitted brake torque. In this example, $W_{in} + W_{out} =$ 11 mm according to Eq. (14), where R_1, R_4, and W_c are given as 9, 30, and 10 mm, respectively. The brake torque is simulated with (W_{in}, W_{out}) varying from (4 mm, 7 mm) to (10 mm, 1 mm). On the horizontal axis, from left to right, W_{in} increases from 4 to 10 mm, and W_{out}, correspondingly, decreases from 7 to 1 mm. It can be seen in Fig. 10 that, if $W_{in} < 5$ mm or $W_{in} > 9$ mm, the brake's transmitted torque T will be relatively low. The brake's transmitted torque, T, reaches a maximum value when (W_{in}, W_{out}) is around (6 mm, 5 mm) and decreases slowly when W_{in} increases. That is, (W_{in}, W_{out}) = (6 mm, 5 mm) would be optimal in terms of the

https://doi.org/10.1017/S0263574707003372 Published online by Cambridge University Press

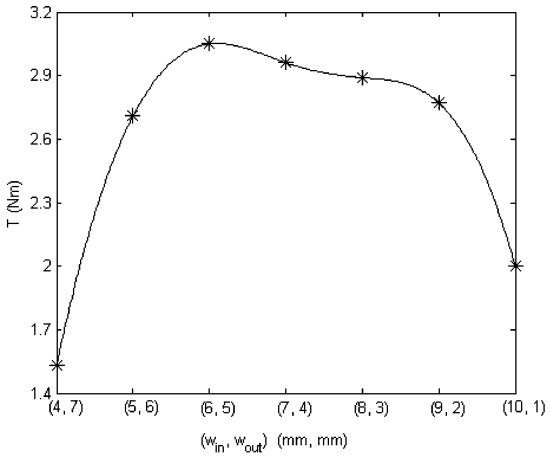

Fig. 10. The brake transmitted torque T with different inner flux path width W_{in} and outer flux path width W_{out}.

maximum brake's transmitted torque. However, parameter sensitivity should also be considered. It can be seen from Fig. 10 that when $W_{\text{in}} < 6$ mm, the generated torque drops sharply with the reduction of W_{in}. Therefore, it has large sensitivity to W_{in}. Whereas, when 6 mm $< W_{\text{in}} <$ 7 mm, the curve is relatively flat and less sensitive to the changes in W_{in} and W_{out}. Therefore, (W_{in}, W_{out}) is preferred to be between (6 mm, 5 mm) and (7 mm, 4 mm).

Once W_{in} and W_{out} are decided, R_2 and R_3 can be computed as follows:

$$R_2 = R_1 + W_{\text{in}} \tag{15}$$

$$R_3 = R_4 - W_{\text{out}}. \tag{16}$$

- *Side steel path thickness, L_{p}*

To reduce the weight and size of the brake, the thickness of the side steel path, L_{p}, is desirable to be as small as possible. However, if the thickness is too small, it will cause magnetic saturation and consequently reduce the magnetic field strength in both shear areas, C_1 and C_2. Therefore, the optimal L_{p} is the smallest value where the magnetic saturation does not happen.

A simulation study of the particular design example which shows how the magnetic field strength at shear areas varies with L_{p} is shown in Fig. 11. From the study, it is observed that, when $L_{\text{p}} < 1.5$ mm, the magnetic field strength in MR fluid gaps will drop significantly with decreasing L_{p}. This is due to the fact that the magnetic saturation starts to happen in the side steel path. Therefore, to reduce weight and at the same time avoid magnetic saturation, a value between 1.5 mm and 2 mm for L_{p} would be optimal for this particular design example.

This analysis gives a general description of the brake design and the parameters' optimization with the assistance of FEA analysis. The objective of parameter optimization is to achieve maximum brake torque with the design constraints, such as mechanical limitations, magnetic saturation, and so on. Note that the parameters' optimizations

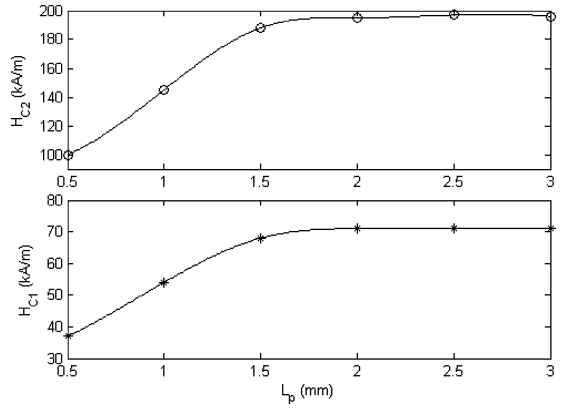

Fig. 11. Magnetic field strength, H, at shear areas, C_1 and C_2, versus the thickness of side steel path, L_{p}.

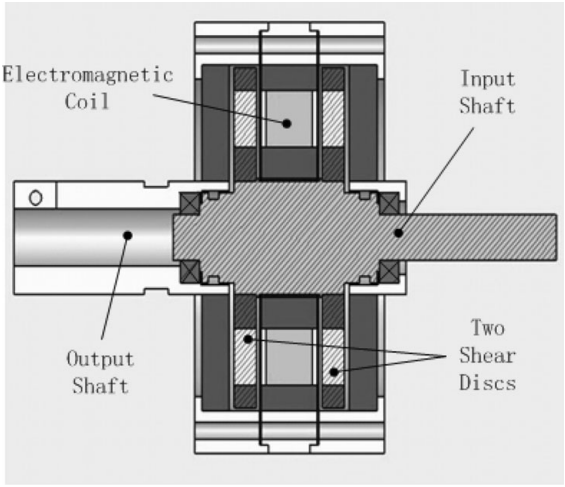

Fig. 12. A cross-sectional view of the MR fluid brake prototype.

are not conducted in sequence. Some design iterations are needed before the most optimal result can be obtained.

3. Realization of a Prototype and Experimental Setup

A CAD drawing of a prototype of the MR fluid brake is shown in Fig. 12. There are an input shaft and an output shaft in the design. The input and the output shafts can rotate independently. Two shearing disks are connected to the input shaft. The transmitted brake torque is passed to the output shaft through the body of the brake. The magnetic coil is placed between the two shear disks to reduce the radial size. Double shear disks also result in more shear area than that of a single one. This design results in a higher torque transmission capacity of the brake. The key specifications of the MR fluid brake prototype are shown in Table II.

An experimental setup as shown in Fig. 13 is also built to test the MR fluid brake prototype. A DC motor is connected to the input shaft of the MR fluid brake to provide the input angular velocity. An encoder is attached to the motor to measure this angular velocity. This will be the shearing angular velocity if the output shaft is fixed. A torque sensor is mounted at the output shaft to measure the transmitted torque. A microcomputer (PC104) is used to control the DC motor based on the feedback from the encoder; and read and

https://doi.org/10.1017/S0263574707003372 Published online by Cambridge University Press

Table II. The key specifications of the MR fluid brake prototype.

Maximum transmitted torque	3.5 Nm
Mechanical dimension	Ø 76 mm × 40 mm
Weight	910 g
Wire diameter	Ø 0.315 mm
Maximum input current	0.8 A
Number of turns	700
Shear gap	1 mm
Effective fluid volume	12 ml
MR fluid	Water-based MR fluid (MRF-241ES)
Magnetic material	Low carbon steel (AISI-1018)
Nonmagnetic material	Aluminum alloy
Sealing	O-ring (rubber)

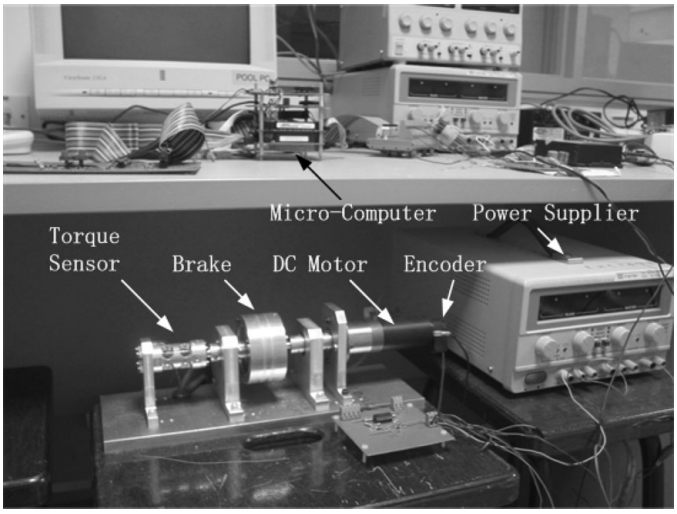

Fig. 13. A picture of the experimental setup.

record the transmitted brake torque from the torque sensor. A DC power supply is used to provide the input current to the magnetic coil of the MR fluid brake.

4. Experimental Results and Discussion

Two experiments were conducted for the MR fluid brake prototype. In the first experiment (Exp 1), the brake velocity was kept constant and the transmitted torque was measured with different currents applied to the magnetic coil of the brake. This experiment was to show the relationship between the brake's transmitted torque and input current. Two velocities (±3 rad/s) were used while the input current varied from 0 to 0.8 A. The negative velocity was used to check the asymmetric property of the brake's transmitted torque.

The experimental results are shown in Fig. 14. From Fig. 14, it can be observed that the maximum transmitted torque is around 3.5 Nm when the applied current is 0.8 A. The brake has a good linear relationship between the transmitted torque and the input current, especially when the current is larger than 0.1 A. The transmitted torque also behaves rather symmetrically. That is, its magnitude remains the same if the velocity of the brake changes its sign (from 3 rad/s to −3 rad/s). When there is no current applied to the

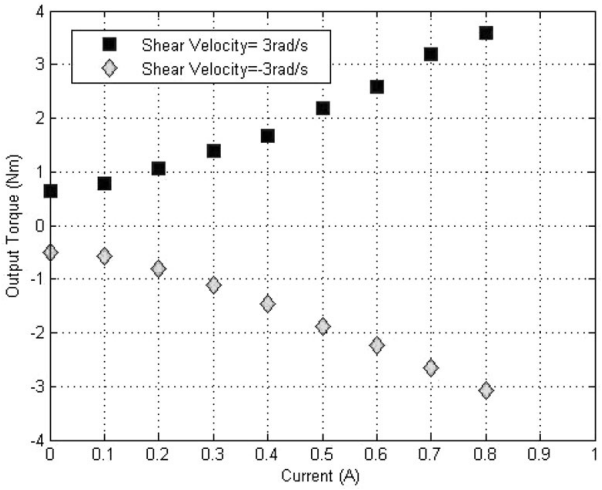

Fig. 14. The transmitted torque of the MR fluid brake prototype plotted against different current values for brake velocity of 3 and −3 rad/s.

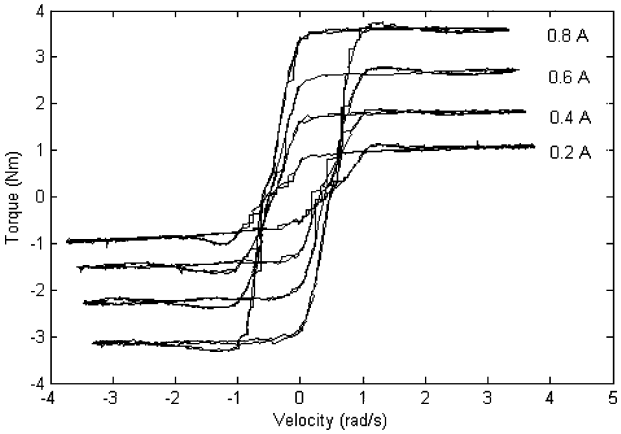

Fig. 15. MR fluid brake's output torque versus velocity for sinusoidal velocity (for brake current 0.2, 0.4, 0.6, and 0.8 A).

brake, the transmitted torque is around 0.55 Nm, which is about 15.7% of the maximum brake torque. This residual torque is mainly attributed to several sources. One of which is the residual shearing torque due to the residual viscosity of the MR fluid. Another important source is due to the friction in the sliding contacts in the brake, for example, at the location where the rubber o-ring used for the MR fluid sealing is situated. Some of these friction sources can be reduced by changing the materials. For the case of the o-ring, as the rubber has relatively large friction coefficient when rubbed against another material, it may be better to use another sealing material such as polymer, which has significantly lower friction coefficient.

In the second experiment (Exp 2), the brake's current was kept constant while a sinusoidal brake velocity was maintained. During the experiment, the transmitted torque was recorded. This experiment was used to study the properties of the MR fluid brake prototype, such as the hysteresis effect, the fluid viscous property, etc.

The sinusoidal brake velocity had an amplitude of 4 rad/s and a frequency of 0.5 Hz. The applied currents were 0.2, 0.4, 0.6, and 0.8 A. The experimental results are presented in Fig. 15. The results show the typical hysteresis behavior

https://doi.org/10.1017/S0263574707003372 Published online by Cambridge University Press

of MR fluid brake. The hysteresis region is within ±1 rad/s. The hysteresis comes from the inherent property of MR fluid brake. It is also observed that the brake torque, beyond the hysteresis region, is almost constant and not dependent on the brake velocity. This means that the viscous component in the dynamics of the MR fluid brake can be neglected.

5. Conclusion

In this paper, a novel MR fluid brake with double shearing disks was proposed, designed, and tested. The brake structure was introduced and Bingham model was used to predict the brake's transmitted torque. General steps for the magnetic circuit design were described. Brake's structural parameters, such as the width of the inner and outer flux path, the thickness of the side steel path, etc., were optimized with the assistance of FEA analysis simulation. A MR fluid brake prototype was manufactured and an experimental system was set up to evaluate the performance of the brake. Experimental results show that a compact MR fluid brake with high transmitted torque was successfully developed.

Acknowledgment

This project is funded by the Academic Research Fund of the National University of Singapore. The authors would like to thank Sateesh Talasila and Dongri Wu for their contributions for this project.

References

1. C.-M. Chew, G.-S. Hong and W. Zhou, "Series Damper Actuator: A Novel Force/Torque Control Actuator," *Proceedings of the IEEE-RAS/RSJ International Conference on Humanoid Robots*, Los Angeles, CA (2004) pp. 533–546.
2. S. J. Dyke and B. F. Spencer Jr., "A Comparison of Semi-Active Control Strategies for the MR Damper," *Proceedings of the Intelligent Information Systems*, Grand Bahama Island, Bahamas (1997) pp. 580–584.
3. M. R. Jolly, J. W. Bender and J. D. Carlson, "Properties and Applications of Commercial Magnetorheological Fluids," *Proceedings of the SPIE 5th International Symposium on Smart Structures and Materials*, San Diego, CA, USA (1998) pp. 262–275.
4. M. Lita, N. C. Popa, C. Velescu and L. N. Vekas, "Investigations of a magnetorheological fluid damper," *IEEE Trans. Magn.*, **40**(2), 469–472 (2004).
5. J.-H. Kim and J.-H. Oh, "Design and Analysis of Rotary MR Damper Using Permanent Magnet," *Proceedings of the 2nd IFAC Conference on Mechatronic Systems*, Berkeley, CA, USA (2002) pp. 899–903.
6. W. H. Li and H. Du, "Design and experimental evaluation of a magnetorheological brake," *Int. J. Adv. Manuf. Technol.*, **21**, 508–515 (2003).
7. G. Pan, H. Matsuhisa and Y. Honda, "Analytical Model of a Magnetorheological Damper and Its Application to the Vibration Control," *Proceedings of the 26th Annual Conference of the IEEE Industrial Electronics Society*, Nagoya, Japan (2000) pp. 1850–1855.
8. C. A. Papadopoulos, "Brakes and clutches using ER fluids," *Mechatronics*, **8**(7), 719–726 (1998).
9. B. M. Kavlicoglu, F. Gordaninejad, C. A. Evernsel, N. Cobanoglu, Y. Liu, A. Fuchs and G. Korol, "A High-Torque Magneto-Rheological Fluid Clutch," *Proceedings of the SPIE Conference on Smart Materials and Structures*, San Diego, CA, USA (2002) pp. 393–400.
10. Lord Corporation, Magneto-Rheological (MR) Fluid/Technology, [online]. Available http://www.lord.com/tabid/3318/Default.aspx, (Sep. 3, 2006).
11. J. D. Carlson, D. F. LeRoy, J. C. Holzheimer and R. H. Marjoram, "Controllable brake," United States Patent, Patent Number: 5,842,547 (1998).
12. B. F. Spencer Jr., S. J. Dyke, M. K. Sain and J. D. Carlson, "Phenomenological model of a magnetorheological damper," *J. Eng. Mech., ASCE*, **123**(3), 230–238 (1997).
13. Ansoft Corporation, Maxwell 2D: 2D Electromagnetic-Field Simulation for High-Performance Electromechanical Design, [online]. Available http://www.ansoft.com/products/em/max2d/, (Dec. 2, 2006).
14. C.-M. Chew, G.-S. Hong and W. Zhou, "Series damper actuator for force/torque control," US Patent Provisional Application, Application No.: 60/469,825 (2004).
15. N. Takesue, H. Asaoka, J. Lin, M. Sakaguchi, G. Zhang and J. Furusho, "Development and Experiments of Actuator Using MR Fluid," *Proceedings of the 2000 IEEE International Conference on Industrial Electronics, Control and Instrumentation*, Nagoya, Japan (2000) pp. 1838–1843.
16. H.-N. Li and Z.-G. Chiang, "Intelligent Algorithm Based Semi-Active Control for MR Damper for Structures," *Proceedings of the Fifth World Congress on Intelligent Control and Automation*, Hangzhou, China (2004) pp. 2428–2432.
17. S. J. Dyke, B. F. Spencer, M. K. Sain and J. D. Carlson, "Modeling and control of magnetorheological dampers for seismic response reduction," *Smart Mater. Struct.*, **5**, 565–575 (1996).
18. R. Stanway, "The Development of Force Actuators Using ER and MR Fluid Technology," *Proceedings of the IEE Colloquium on Actuator Technology: Current Practice and New Developments*, London, UK (1996) pp. 6/1–6/5.
19. Lord Corporation, Engineering Note: Magnetic Circuit Design, [online]. Available http://literature.lord.com/root/other/rheonetic/Magnetic_Circuit_Design.pdf (Sep. 3, 2005).
20. J. H. Yoo and N. M. Wereley, "Design of a high-efficiency magnetorheological valve," *J. Intell. Mater. Syst. Struct.*, **13**(10), 679–685 (2002).
21. W. H. Li, H. Du and N. Q. Guo, "Finite element analysis and simulation evaluation of a magnetorheological valve," *Int. J. Adv. Manuf. Technol.*, **21**(6), 438–445 (2003).
22. J. An and D. S. Kwon, "Modeling of MR actuator including magnetic hysteresis," *J. Intell. Mater. Syst. Struct.*, **14**, 541–550 (2003).